Magnetic properties of a spin-orbit entangled $J_{\text{eff}} = \frac{1}{2}$ three-dimensional frustrated rare-earth hyperkagome material

B. Sana,[1] M. Barik,[1] M. Pregelj,[2,3] U. Jena,[1] M. Baenitz,[4] J. Sichelschmidt,[4] K. Sethupathi,[1,5] and P. Khuntia[1,5,*]

[1]*Department of Physics, Indian Institute of Technology Madras, Chennai 600036, India*

[2]*Jožef Stefan Institute, Jamova cesta 39, 1000 Ljubljana, Slovenia*

[3]*Faculty of Mathematics and Physics, University of Ljubljana, Jadranska ulica 19, 1000 Ljubljana, Slovenia*

[4]*Max Planck Institute for Chemical Physics of Solids, Nöthnitzer Strasse 40, 01187 Dresden, Germany*

[5]*Quantum Centre of Excellence for Diamond and Emergent Materials, Indian Institute of Technology Madras, Chennai 600036, India*

(Received 14 April 2023; revised 24 August 2023; accepted 18 September 2023; published 11 October 2023)

The interplay between competing degrees of freedom can stabilize nontrivial magnetic states in correlated electron materials. Frustration-induced strong quantum fluctuations can evade long-range magnetic ordering, leading to exotic quantum states such as spin liquids in two-dimensional spin lattices such as triangular and kagome structures. However, experimental realization of dynamic and correlated quantum states is rare in three-dimensional (3D) frustrated magnets, wherein quantum fluctuations are less prominent. Here, we report the crystal structure, magnetic susceptibility, electron spin resonance, and specific heat studies accompanied by crystal electric field calculations on the 3D frustrated magnet $Yb_3Sc_2Ga_3O_{12}$. In this material, Yb^{3+} ions form a three-dimensional network of corner-sharing triangles known as a hyperkagome lattice without any detectable antisite disorder. Our thermodynamic results reveal a low-energy state with $J_{\text{eff}} = \frac{1}{2}$ degrees of freedom in the Kramers doublet state. The zero-field-cooled and field-cooled magnetic susceptibilities taken at 0.001 T rule out the presence of spin freezing down to 1.8 K. The Curie-Weiss fit of magnetic susceptibility at low temperature yields a small and negative Curie-Weiss temperature, indicating the presence of a weak antiferromagnetic interaction between $J_{\text{eff}} = \frac{1}{2}$ (Yb^{3+}) moments. The Yb-electron spin resonance displays a broad line of asymmetric shape consistent with the presence of considerable magnetic anisotropy in $Yb_3Sc_2Ga_3O_{12}$. The crystal electric field calculations suggest that the ground state is well separated from the excited states, which are in good agreement with experimental results. The absence of long-range magnetic ordering inferred from specific heat data indicates a dynamic liquidlike ground state at least down to 130 mK. Furthermore, zero-field specific heat shows a broad maximum around 200 mK, suggesting the presence of short-range spin correlations in this three-dimensional frustrated antiferromagnet.

DOI: 10.1103/PhysRevB.108.134413

I. INTRODUCTION

Geometrically frustrated magnets have drawn significant attention due to their emergent magnetic phenomena arising from competing interactions and quantum fluctuations [1–4]. Two-dimensional (2D) frustrated magnets are prime contenders to host exotic quantum states with fractional quantum numbers following the seminal proposal of a quantum spin liquid state on a triangular lattice antiferromagnet by Anderson [5]. Frustrated magnets with next-nearest-neighbor exchange interaction, bond-dependent Ising interactions, and magnetic anisotropy are ideal candidates in this context [2,6]. A quantum spin liquid (QSL) is characterized by the absence of long-range magnetic order despite strong exchange interaction between spins, the absence of the local order parameter, and spins not freezing down to absolute zero. The spins maintain a highly entangled state in the QSL state, which harbors exotic fractional excitations such as spinons and Majorana fermions, which are essential ingredients for future quantum information processing [3,4,6–9]. Geometrically frustrated triangular, kagome, and hyperkagome lattices, wherein frustration-induced strong quantum fluctuations are at play, offer a promising platform for the experimental realization of QSL. The identification of associated nontrivial quasiparticles and their interactions in the QSL state is an attractive track in quantum condensed matter. The exotic excitations in the QSL state are completely different from spin-wave excitations observed in conventional magnets with static order [1,2,6]. There are reports on quite a good number of promising two-dimensional quantum spin liquid candidates; however, a very few three-dimensional (3D) quantum spin liquids have been studied so far [7,8,10–31].

Remarkably, an excellent three-dimensional lattice to realize the exotic magnetic ground state is rare-earth pyrochlore oxides, $R_2B_2O_7$, where R^{3+} and B^{4+} are generally trivalent rare-earth and tetravalent transition metal ions, respectively. In this rare-earth magnet family, the ground state of some Kramers ion is a well-separated crystal electric field doublet with interacting $J_{\text{eff}} = \frac{1}{2}$ pseudospins at low temperatures. Depending upon how the ground state doublet transforms under time-reversal symmetry and local D_{3d} crystal field

*pkhuntia@iitm.ac.in

symmetry of the rare-earth site, this pyrochlore can harbor a dipole-octupole ground state doublet, which supports an exotic U(1) quantum spin liquid ground state [32,33]. For example, in the quantum spin liquid candidate $Ce_2Zr_2O_7$, the x and z components of pseudo-spin-$\frac{1}{2}$ degrees of freedom of the Ce^{3+} ion behave as dipoles, whereas only the y component behaves as an octupole under the time-reversal symmetry and lattice symmetry [33]. Coupling between the magnetic field and spinons enables us to control spinon excitations by applying an external magnetic field in this octupolar spin liquid candidate [32]. Among 3D spin liquid candidates, the three-dimensional network of corner-sharing triangles known as the hyperkagome lattice has recently drawn significant attention due to its rich ground state properties. One exemplar is $PbCuTe_2O_6$, wherein spin $S = \frac{1}{2}$ transition metal Cu^{2+} ions constitute a hyperkagome lattice. The local probe techniques nuclear magnetic resonance and muon spin resonance revealed a dynamic ground state down to 20 mK in this hyperkagome lattice [24,25]. Diffusive continua in magnetic excitation spectra revealed by neutron scattering experiment provide strong evidence of fractional spinon excitations in this 3D frustrated magnet [26]. Another geometrically frustrated effective spin $J_{\text{eff}} = \frac{1}{2}$ 3D spin liquid candidate is $Na_4Ir_3O_8$ [34,35]. Despite strong antiferromagnetic interaction between Ir^{4+} ($J_{\text{eff}} = \frac{1}{2}$) moments, which was confirmed by a large Curie-Weiss temperature of -650 K, there is no sign of magnetic ordering down to a few kelvin. A theoretical study proposed the existence of a Z_2 quantum spin liquid state in the quantum regime (i.e., small spin) of the hyperkagome lattice $Na_4Ir_3O_8$ [36]. However, a small splitting of zero-field-cooled (ZFC) and field-cooled (FC) magnetization data suggests the role of static moments below 7 K, which imposes a strong constraint on the unambiguous identification of the spin liquid ground state in this material [37]. The rare realization of the 3D QSL is due to the fact that the Neél order or spin freezing is energetically favorable over the QSL state in the case of a 3D frustrated spin lattice for $S > \frac{1}{2}$. However, frustration-induced strong quantum fluctuations in the $S = \frac{1}{2}$ or $J_{\text{eff}} = \frac{1}{2}$ system make it a potential candidate to host a dynamic ground state [5,30,38]. It is highly relevant to explore whether the disorder interaction or exchange anisotropy or lattice imperfections account for spin freezing in this type of 3D spin liquid candidate.

In this context, synthesis and investigation of three-dimensional frustrated spin-lattices, wherein the interplay between competing degrees of freedom and spin correlations could lead to exotic quantum states, are highly needed. Considerable efforts have been devoted to this topic; for instance, a disorder-free $4f$-based hyperkagome lattice, wherein spin frustration and anisotropic interactions governed by spin-orbit interaction stabilize an effective low-energy $J_{\text{eff}} = \frac{1}{2}$ ground state, offers an alternate route for the realization of elusive 3D spin liquids. The hyperkagome lattice-based material $Li_3Yb_3Te_2O_{12}$, where Yb^{3+} spins decorate a corner-shared frustrated triangular network, shows a dynamical ground state down to 38 mK temperature [39]. Magnetic Yb^{3+} ions show short-range spin correlations with $J_{\text{eff}} = \frac{1}{2}$ degrees of freedom in the ground state. One promising family of compounds to study the rare-earth hyperkagome lattice is lanthanide garnets with the general formula $R_3A_2X_3O_{12}$, where R = rare-earth elements; A = Ga, Sc, In, Te; and X = Ga, Al, Li [40]. In this series, rare-earth ions occupying two interpenetrating frustrated hyperkagome networks have a rich potential to harbor myriads of novel physical phenomena. For example, the antiferromagnetic spin correlation and local magnetic anisotropy lead to a nontrivial magnetic structure with a long-range hidden order state in $Gd_3Ga_5O_{12}$ [41,42]. Spin clusters behave like a single object due to strong spin correlation, and these spin clusters show long-range nondipolar order, although the individual spin maintains a dynamic liquidlike state [41,43]. On the other hand, emergent magnetic behavior with short-range spin correlations was observed in the $J_{\text{eff}} = \frac{1}{2}$ Yb^{3+} containing garnet $Yb_3Ga_5O_{12}$ [44]. The specific heat data show a λ-like anomaly which was attributed to long-range magnetic order [45]. However, muon spin resonance and Mössbauer spectroscopy measurements indicate the absence of long-range magnetic order [45,46]. In the opposite scenario, an antiferromagnetically ordered state develops below in the subkelvin temperature range in other members of the garnet family [47,48]. Although there are several studies on gallium garnets, the magnetic properties of scandium gallium garnets have yet to be investigated. A recent study on $R_3Sc_2Ga_3O_{12}$ (R = Tb, Dy, Ho) revealed that most of these garnets undergo a long-range antiferromagnetic ordering state at low temperature [40]. The magnetic properties of this family of materials is highly sensitive to external stimuli such as chemical pressure, temperature, and an applied magnetic field. It is pertinent to test the effect of external perturbations such as nonmagnetic and magnetic ions on the anisotropy, exchange interactions, and hence the underlying spin Hamiltonian in this interesting class of three-dimensional frustrated magnets. The magnetic moment of the Yb^{3+} ion is relatively weak compared to that of other R^{3+} ions. Because Yb^{3+} is a Kramers ion, a combination of crystal electric field and spin-orbit coupling could lead to a low-energy $J_{\text{eff}} = \frac{1}{2}$ state in the Yb variant of this promising garnet series. This suggests that $Yb_3Sc_2Ga_3O_{12}$ has special interest in the search for a spin-orbit-driven ground state.

Here, we report the synthesis, magnetization, electron spin resonance (ESR), and thermodynamic studies for the garnet $Yb_3Sc_2Ga_3O_{12}$, wherein Yb^{3+} ions constitute a three-dimensional frustrated corner-sharing network of triangles, namely, a hyperkagome spin-lattice. The combination of crystal electric field and spin-orbit coupling stabilizes the low-energy pseudo-spin $J_{\text{eff}} = \frac{1}{2}$ state of the Kramers doublets of the Yb^{3+} ion at low temperature. The absence of ZFC-FC splitting of magnetic susceptibility at 0.001 T rules out spin freezing down to 1.8 K in this material. The low-temperature Curie-Weiss fit yields a weak antiferromagnetic interaction between Yb^{3+} ($J_{\text{eff}} = \frac{1}{2}$) moments in the spin lattice. The magnetic ground state is investigated via thermodynamic measurements, which reveal that this garnet remains in a quantum disordered ground state at least down to 130 mK. The specific heat in zero field shows a broad maximum around 200 mK, implying the presence of short-range spin correlations in this three-dimensional frustrated spin lattice. The crystal electric field calculations infer that the lowest Kramers ground state is well separated from the excited states and imply considerable magnetic anisotropy, which is consistent with experiments.

TABLE I. Structural parameters of $Yb_3Sc_2Ga_3O_{12}$ determined from the Rietveld refinement of powder x-ray diffraction pattern taken at room temperature using the FULLPROF software. The space group is $Ia\bar{3}d$, and cell parameters are $a = b = c = 12.391$ Å, $\alpha = \beta = \gamma = 90°$, and $\chi^2 = 5.4$.

Atoms	Wyckoff	x	y	z	Occupancy
Ga	24*d*	0	0.25	0.375	1
Sc	16*a*	0	0	0	1
Yb	24*c*	0	0.25	0.125	1
O	96*h*	−0.0316	0.0561	0.1508	1

II. EXPERIMENTAL DETAILS

A polycrystalline sample of $Yb_3Sc_2Ga_3O_{12}$ was prepared via the sol-gel method. The rare-earth oxide Yb_2O_3 was preheated at 900 °C for 6 h prior to use to remove moisture and carbonates. Stoichiometric amounts of Yb_2O_3 (Alfa Aesar, 99.998%), Sc_2O_3 (Alfa Aesar, 99.9%), and Ga_2O_3 (Alfa Aesar, 99.999%) were dissolved in hot nitric acid separately in three beakers. The concentration of these acidic solutions was reduced by adding and evaporating deionized water. These three nitrate solutions were then mixed together, and polyethylene glycol was added to the solution. This solution was kept between 90 °C and 120 °C on a magnetic stirrer for several hours. The gel was dried, yielding ashlike powders, which were preheated at 800 °C for 6 h, and finally, a white polycrystalline sample was obtained. This was followed by heat treatment of the resulting sample at 1000 °C, 1100 °C, and 1200 °C for a few days. Before each heat treatment, the sample was ground and pelletized to ensure better homogeneity. A Rigaku x-ray diffractometer was deployed to check the phase purity at room temperature using Cu $K\alpha$ radiation. A Quantum Design superconducting quantum interference device vibrating-sample magnetometer was used to perform magnetization measurements in the temperature range $1.8 \leqslant T \leqslant 350$ K under magnetic field of $0 \leqslant \mu_0 H \leqslant 5$ T. ESR experiments were performed at 9.4 GHz (X-band frequency) on a high-quality polycrystalline sample of $Yb_3Sc_2Ga_3O_{12}$ material for temperatures down to 4 K. Specific heat measurements were carried out with a Quantum Design physical properties measurement system (PPMS) in magnetic fields up to 7 T and in the temperature range $1.8 \leqslant T \leqslant 200$ K. The low-temperature specific heat measurement down to 130 mK was performed using a dilution refrigerator setup attached to a Dynacool PPMS from Quantum Design. Fitting and modeling of the crystal electric field (CEF) effects were preformed using PHI software [49].

A. Crystal structure

For the Rietveld refinement of the $Yb_3Sc_2Ga_3O_{12}$ hyperkagome material, initial crystallographic parameters were taken from its isostructural compound $Gd_3Sc_2Ga_3O_{12}$, which crystallizes in the cubic space group $Ia\bar{3}d$ [40]. Rietveld refinement was performed using the FULLPROF SUITE on powder x-ray diffraction (XRD) data recorded at room temperature, and the refined parameters are $R_p = 8.3\%$, $R_{wp} = 9.2\%$, and $\chi^2 = 5.4$ [50] (see Fig. 1). Refined atomic coordinates are presented in Table I. The lattice constant a turned out to be

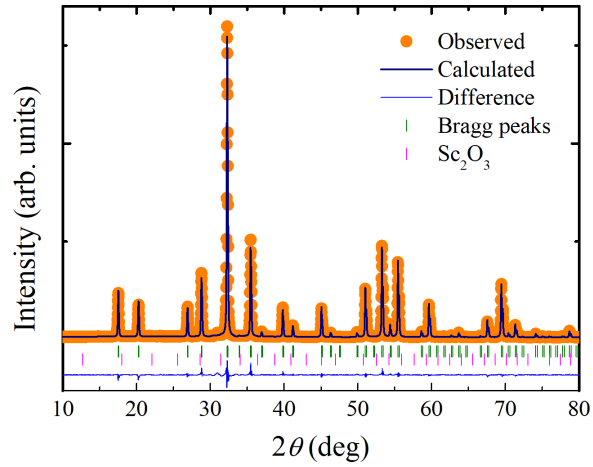

FIG. 1. Rietveld refinement of powder XRD data taken at room temperature.

12.391 Å, which is smaller than that found in other rare-earth-based isostructural compounds ($R_3Sc_2Ga_3O_{12}$, R = Gd, Tb, Dy, and Ho) [40]. This reduction is due to the small ionic radius of the Yb^{3+} ion compared to other rare-earth ions. A tiny impurity peak at around $2\theta \approx 31°$ indicates a minor (1.5%) phase of unreacted Sc_2O_3 which is nonmagnetic, and its impact on the overall magnetic behavior of the oxide is negligible. The crystal structure was drawn by using VESTA, as shown in Fig. 2(a) [51]. The two interpenetrating

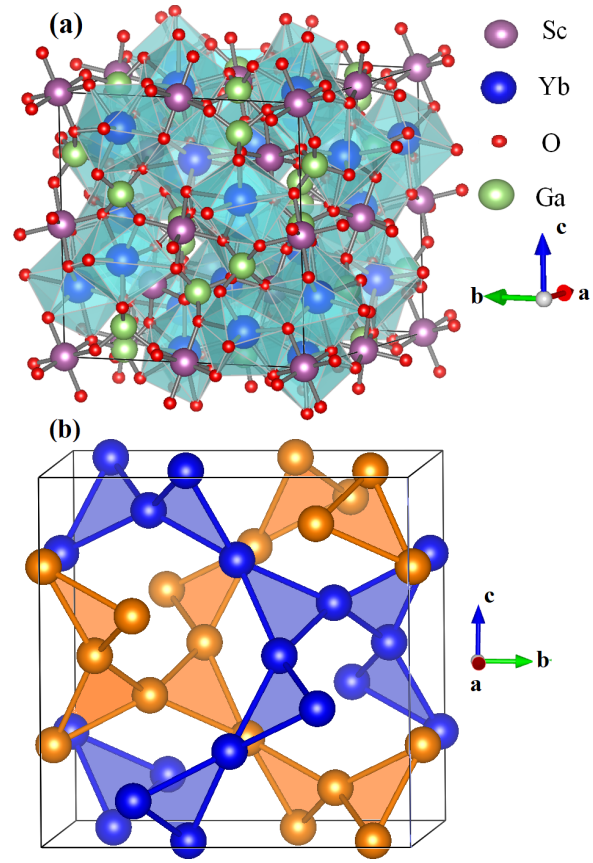

FIG. 2. (a) Crystal structure of $Yb_3Sc_2Ga_3O_{12}$. (b) Two interpenetrating hyperkagome networks of Yb^{3+} ions.

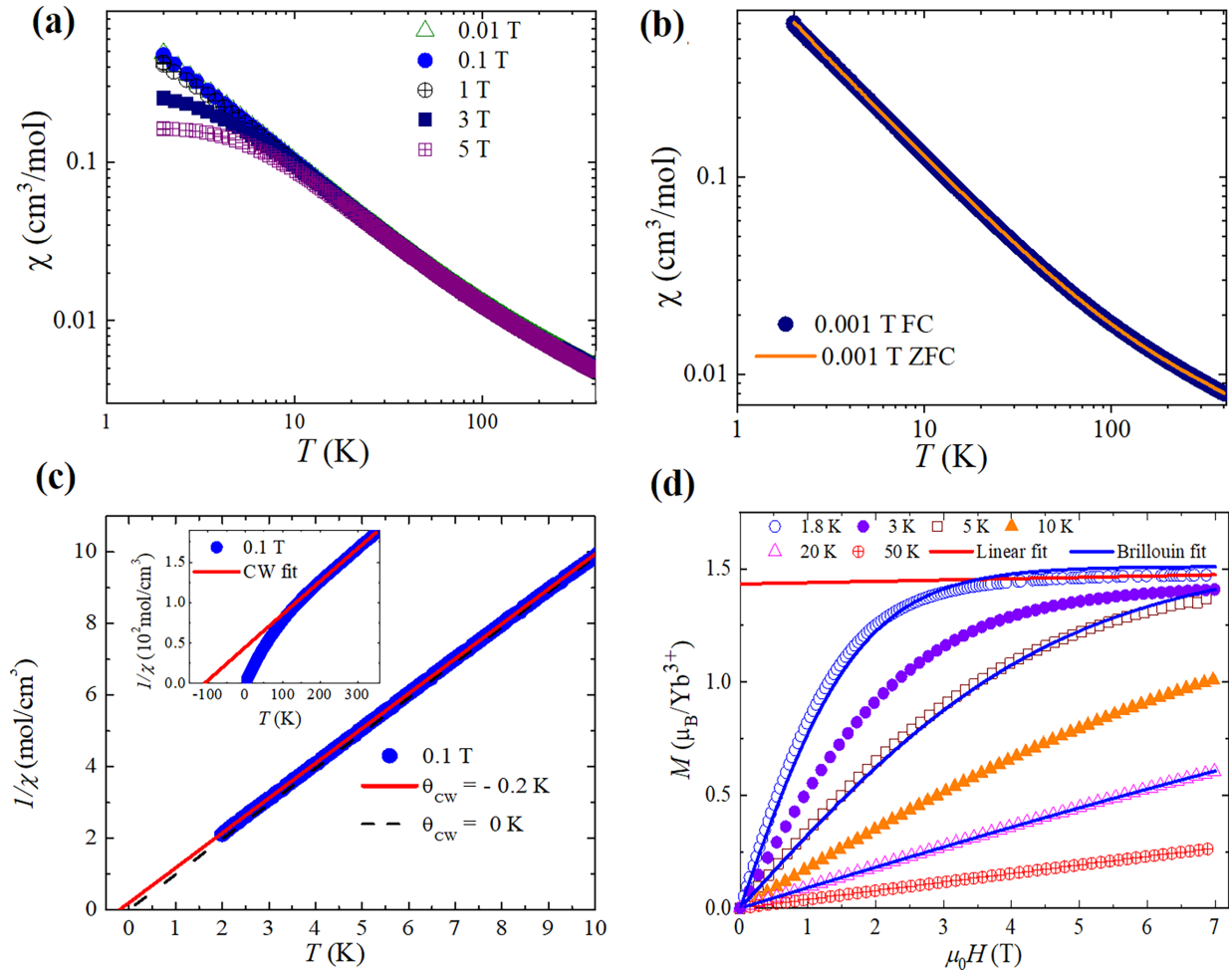

FIG. 3. (a) The temperature dependence of magnetic susceptibility in different applied magnetic fields reordered in the ZFC mode. (b) The temperature dependence of zero-field-cooled and field-cooled magnetization data taken at 0.001 T. (c) Curie-Weiss fit to inverse susceptibility data taken at 0.1 T. Blue solid circles denote experimental data, whereas solid and dashed lines denote Curie-Weiss fits. The inset shows the same fit in the higher temperature range $200 \leqslant T \leqslant 350$ K. (d) Magnetic isotherms at different temperatures. Magnetization taken in ramping up and down modes remain identical, which adds further credence to the absence of spin glass physics. From the slope of the linear fit (solid red line) to high-field data taken at 1.8 K a Van Vleck contribution to susceptibility was extracted. Blue lines are Brillouin fits for $J_{\text{eff}} = \frac{1}{2}$ at different temperatures.

hyperkagome networks made of Yb^{3+} ions are shown in Fig. 2(b). Each Yb atom is surrounded by eight oxygen atoms, forming a YbO_8 polyhedron. Four of them are at a distance 2.4 Å, and the rest are at 2.455 Å, forming a dodecahedron structure. The nearest-neighbor Yb-Yb bond length is 3.794 Å, whereas the second-nearest-neighbor bond is 5.796 Å. There are two Yb-O-Yb bridging exchange paths between two nearest-neighbor Yb atoms, both making an angle of 102.8°. The presence of corner-shared triangles might induce magnetic frustration in this material.

B. Magnetization

Magnetic susceptibility measurements were carried out in the temperature range $1.8 \leqslant T \leqslant 350$ K under several applied magnetic fields. Figure 3(a) shows the temperature dependence of magnetic susceptibility data taken in applied magnetic fields in the range $0.01 \leqslant \mu_0 H \leqslant 5$ T. The absence of an anomaly in the magnetic susceptibility data indicates that there is no magnetic phase transition down to 1.8 K. The absence of any splitting in ZFC and FC data taken at 0.001 T rules out spin freezing down to 1.8 K [see Fig. 3(b)]. This is further confirmed by the absence of hysteresis in the magnetization isotherm taken at 1.8 K (see Fig. 1(b) in the Supplemental Material [52]). High-temperature inverse susceptibility data were well reproduced using the Curie-Weiss formula $\chi(T) = \frac{C}{T-\theta_{\text{CW}}}$ in the temperature range $200 \leqslant T \leqslant 350$ K [see the inset of Fig. 3(c)]. The fit yields a negative $\theta_{\text{CW}} \approx -114 \pm 1$ K, which is attributed to crystal electric field effects, and a change in the population of crystal electric field levels can induce strong curvature in the $\chi^{-1}(T)$ curve (here, below 150 K). The Curie-Weiss constant C turns out to be 2.49 cm^3 K/mol, resulting in an effective moment $\mu_{\text{eff}} = 4.5\mu_{\text{B}}$, close to the free ion effective moment ($4.54\mu_{\text{B}}$) of the Yb^{3+} ($4f^{13}$, $^2F_{7/2}$; $J = 7/2$) ion ($g\sqrt{J(J+1)}\mu_{\text{B}}$, g Landé factor). In the presence of CEF, the eightfold-degenerate ground state

TABLE II. Comparison of the lattice parameter, Curie-Weiss temperature θ_{CW}, and the magnetic ordering temperature of scandium garnet, $R_3Sc_2Ga_3O_{12}$.

	R				
	Gd	Tb	Dy	Ho	Yb
a (Å)	12.573	12.539	12.502	12.475	12.391
θ_{CW} (K)	−2.2	−1.2	−0.8	−2.9	−0.2(1)
T_N(K)	<0.4	0.7	1.11	2.4	<0.13
Ref.	[40]	[40]	[40]	[40]	this work

of the Yb^{3+} ion splits into four Kramers doublets [53]. In this scenario, the Curie-Weiss temperature obtained from the high-temperature fit is inadequate to describe the magnetic exchange interaction because some of the Kramers doublets with higher energy might be populated and Curie-Weiss temperature is dominated by these crystal field levels (see the Supplemental Material [52]). The deviation of the temperature dependence of inverse magnetic susceptibility around 150 K indicates the presence of another energy scale of interaction between Yb^{3+} moments at low temperature. In principle, the correlation between $4f$ moments develops at very low temperature, and this correlation, accompanied by competing degrees of freedom, accounts for the ground state properties in rare-earth-based frustrated quantum magnets [23]. In order to get an idea about the exchange interaction between Yb^{3+} moments, we fit the temperature dependence of the inverse magnetic susceptibility with the Curie-Weiss formula in the temperature range $1.8 \leqslant T \leqslant 10$ K [see Fig. 3(c)]. A weak Curie-Weiss temperature of −0.2(1) K and an effective moment of $2.9(3)\mu_B$ were obtained from the best fit (see Fig. 1(a) in the Supplemental Material [52]). The negative and small Curie-Weiss temperature indicates the presence of weak antiferromagnetic interaction between the Yb^{3+} spins. A comparison of the Curie-Weiss temperature, lattice parameter, and magnetic ordering temperature of the isostructural scandium garnets is presented in Table II. A small Curie-Weiss temperature is usually found in rare-earth magnets [23,44,54]. From the value of the effective moment, the g factor turns out to be 3.3(3). The reduced effective moment compared to that expected for the Yb^{3+} free ion is attributed to the $J_{eff} = \frac{1}{2}$ Kramers doublet ground state at low temperatures [23,54–56]. Figure 3(d) depicts the magnetization isotherms at different temperatures. At higher field and low temperature, magnetization increases linearly due to the Van Vleck paramagnetism. From the linear behavior of the curve, we have determined a Van Vleck term of $\chi_{vv} = 0.0059\mu_B/T = 0.003$ cm^3/mol. The saturation magnetic moment was found to be $1.43\mu_B/Yb^{3+}$ after subtracting the Van Vleck term, which is consistent with $M_s = g_{avg}J_{eff}(1/2)\mu_B$. The fit of the $M(H)$ data taken at 1.8 K with the Brillouin function also yields a g value of ≈3.0(2), close to the value obtained from the Curie-Weiss fit to low-temperature inverse magnetic susceptibility data [see Fig. 3(d)]. However, the Brillouin fit deviates slightly, probably indicating the presence of weak antiferromagnetic interactions between Yb^{3+} moments at low temperature. The data taken at 20 K are well fitted with the Brillouin function as the material is in the paramagnetic region. In these fittings, the J value was fixed to $\frac{1}{2}$ to account for the $J_{eff} = \frac{1}{2}$ ground state. The dipolar interaction energy and dipolar Curie-Weiss temperature were deduced from the formulas $E_d = (\frac{8}{\sqrt{6}})^3 \frac{(g\mu_B S)^2}{a^3}$ and $\theta_{CW}^{dip} = 32\pi \frac{(g\mu_B)^2 S(S+1)}{3a^3 k_B}$, which were used for the isostructural compound $Yb_3Ga_5O_{12}$ [56]. Here, a is the lattice parameter. E_d and θ_{CW}^{dip} turn out to be 31 and 90 mK, respectively. Different magnetic interactions contribute additively to the Curie-Weiss temperature (i.e., $\theta_{CW} = \theta_{CW}^{dip} + \theta_{CW}^{ex}$) [57,58]; the Curie-Weiss temperature due to exchange interaction (i.e., θ_{CW}^{ex}) turns out to be $\sim -0.3(1)$ K. The exchange interaction J_{ex} could be obtained using the formula $J_{ex} = \frac{3k_B\theta_{CW}^{ex}}{zS(S+1)}$ [59], where z represents the number of nearest neighbors. Using $z = 4$ for the hyperkagome structure and effective spin $S \equiv J_{eff} = \frac{1}{2}$, we found $J_{ex} = -0.3(1)$ K. The presence of weak exchange interaction is typical in rare-earth oxides and is attributed to the fact that $4f$ orbitals of rare-earth ions are localized and well shielded, yielding weak overlap between two nearest-neighbor orbitals.

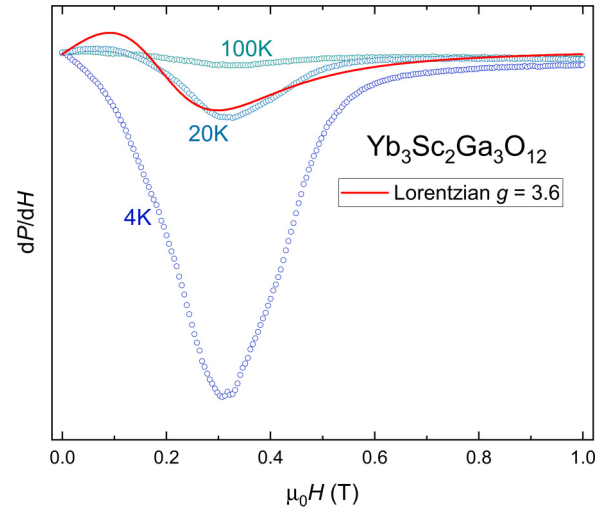

FIG. 4. ESR spectra of a polycrystalline sample of $Yb_3Sc_2Ga_3O_{12}$ at indicated temperatures and X-band frequency. dP/dH denotes the first field derivative of the absorbed microwave power. The line denotes fitting of the 20 K data with a Lorentzian shape with a corresponding g value of 3.6.

C. Electron spin resonance

ESR is an excellent low-energy local probe to determine the effective g factor as well as to characterize single-ion and exchange anisotropies, which are crucial to establish a realistic microscopic Hamiltonian of frustrated quantum materials. It was shown that ESR can shed microscopic insight into the QSL state and associated exotic excitations in frustrated magnets with significant spin-orbit interaction [60]. Figure 4 depicts ESR signals of a polycrystalline sample of $Yb_3Sc_2Ga_3O_{12}$ at representative temperatures. Due to the rather large linewidth, Yb containing secondary phases may be excluded as the origin of the signal. We describe the line by a Lorentzian shape that also includes the negative resonance field component due to the influence of the counterrotating component of the linearly polarized microwave field. Such a

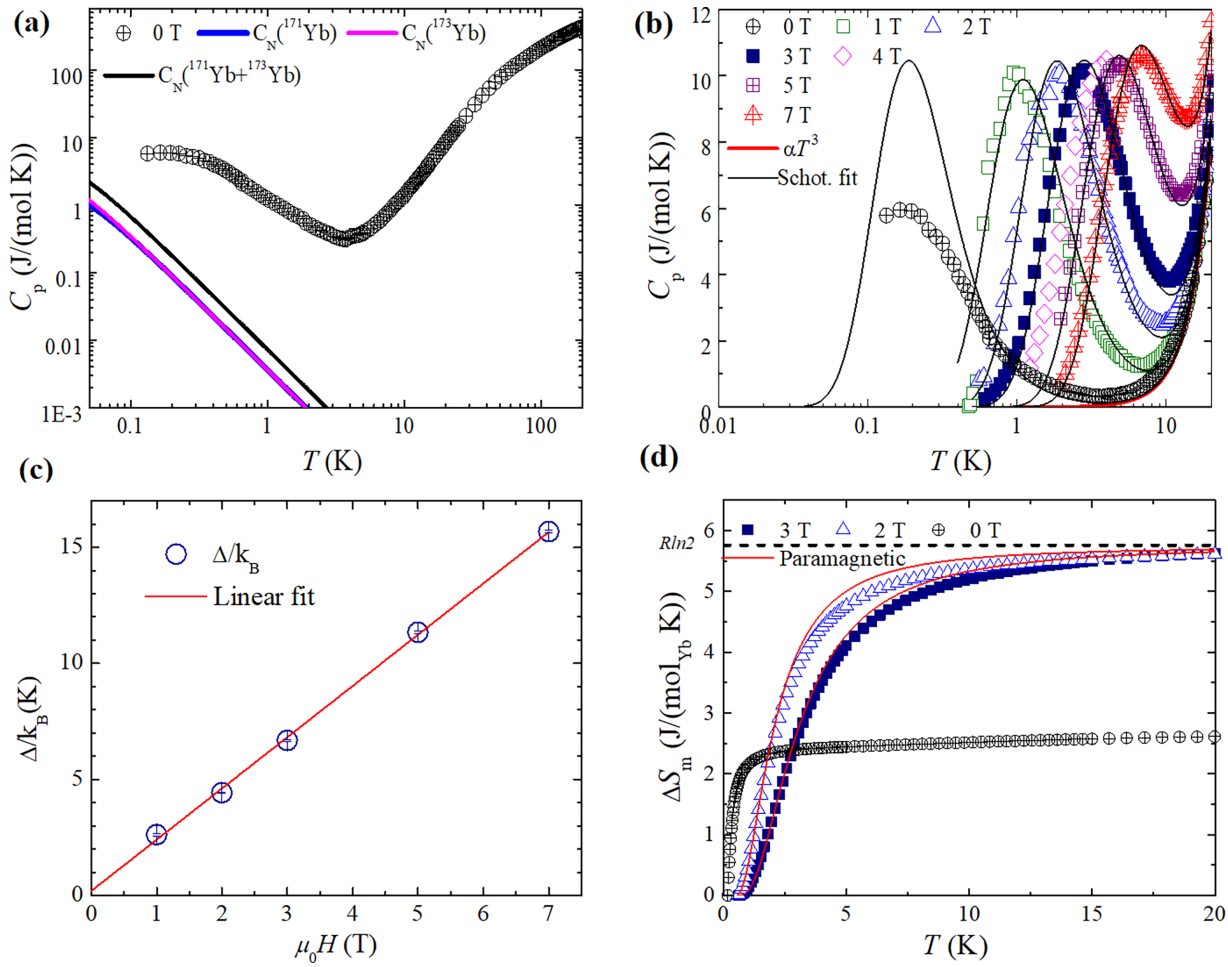

FIG. 5. (a) Temperature dependence of specific heat (0.13 K $\leqslant T \leqslant$ 200 K) for $Yb_3Sc_2Ga_3O_{12}$ in zero field. The nuclear Schottky contributions to the specific heat for 3 × 0.1431 mol of ^{171}Yb and 3 × 0.1613 mol of ^{173}Yb are denoted by blue and pink lines, respectively. (b) Low-temperature specific heat (0.13 K $\leqslant T \leqslant$ 20 K) in several applied magnetic fields. Corresponding Schottky fits are denoted by black solid lines. Phonon contributions were taken into account while fitting by adding the αT^3 term indicated by the red solid line. (c) Linear behavior of the Schottky gap Δ/k_B with applied magnetic field; the solid red line is a linear fit. From the slope of the fit we found $g = 3.3(1)$, and the intercept turns out to be 0.2(1) K. (d) Magnetic entropy in applied magnetic fields. Corresponding paramagnetic entropy in applied fields is denoted by red solid lines. Experimental entropy is slightly smaller than the ideal paramagnet, which suggests the existence of a small exchange interaction and/or magnetic frustration. For higher fields, it saturates at 97% of the full entropy ($R \ln 2$) expected for magnetic materials with $J_{\text{eff}} = \frac{1}{2}$ degrees of freedom, consistent with magnetization results.

fit yields, for the 20 K data, a resonance field of 0.18 T (which corresponds to a g value of 3.6) and a linewidth of 0.2 T. The large linewidth compared to the resonance field poses a strong constraint on precisely quantifying the temperature dependences of ESR parameters in the measured temperature range $4 \leqslant T \leqslant 175$ K. Nevertheless, a clear tendency of line broadening towards low and high temperatures as well as a downshift of the resonance field towards low temperature can be identified. This behavior may be due to a relaxation via the first excited crystal electric field level of the Yb^{3+} ion and the slowing down of Yb^{3+} spin fluctuations in the low-temperature regime [61]. The strong deviation from a symmetric Lorentzian line shape points to off-diagonal terms in the dynamic susceptibility. This is typical for systems with anisotropic spin lattices and becomes even more pronounced when very broad lines are present [62]. A detailed discussion along these lines would be reasonable only if ESR data of single crystals were available.

D. Specific heat

Specific heat provides an excellent probe to gain insights into the ground state properties of this rare-earth hyperkagome lattice. Figure 5(a) shows the specific heat as a function of temperature down to 130 mK in zero field. The absence of any anomaly in zero field thus confirms the evasion of long-range magnetic ordering down to at least 130 mK despite a weak antiferromagnetic exchange interaction between $J_{\text{eff}} = \frac{1}{2}$ moments. The peak in specific heat due to the nuclear Schottky effect usually occurs below 10^{-2} K [63–65]. To calculate the expected nuclear specific heat contribution, we have considered the fact that the natural abundances of ^{171}Yb ($I = 1/2$) and ^{173}Yb ($I = 5/2$) are 14.31% and 16.13%, respectively [see Fig. 5(a)] [66–68]. The energy separation between two consecutive levels for ^{171}Yb and ^{173}Yb are 63.9 and 17.55 mK, respectively, which are taken from values reported for the isostructural compound $Yb_3Ga_5O_{12}$ [66]. The quadrupole coupling constant P (see Eq. (3) in the Supplemental Material

TABLE III. CEF parameters (in meV) for the CEF Hamiltonian in Eq. (3) and g factors of the ground state for the CEF model.

B_2^0	B_2^2	B_4^0	B_4^2	B_4^4	B_6^0	B_6^2	B_6^4	B_6^6	g_x	g_y	g_z
−0.06229	0.3036	0.08183	−0.04343	−0.03914	0.0000166	−0.01486	0.02468	−0.009285	2.93	2.25	4.24

[52]) is zero for ^{171}Yb and nonzero for ^{173}Yb. However, we have neglected the quadrupole term in our calculation (see the Supplemental Material for details) due to its insignificant impact on shifting the Schottky peak. Upon the application of an external magnetic field, a broad maximum appears at low temperature in specific heat data of $Yb_3Sc_2Ga_3O_{12}$ that shifts significantly to higher temperature upon increasing magnetic field [see Fig. 5(b)], which is associated with the electronic Schottky anomaly originating from the Zeeman splitting of the lowest-lying energy levels. To evaluate the Schottky contribution, field-dependent $C_p(H)$ data were fitted with the equation $C_p = C_L + C_S(\Delta)$ [see Fig. 5(b)], where $C_S(\Delta)$ is the specific heat with an energy level splitting Δ due to an applied magnetic field $\mu_0 H$ [69,70]. C_L is the lattice contribution to the specific heat. We fitted the low-temperature zero-field specific heat data in the temperature range $4 \leqslant T \leqslant 22$ K with the equation relevant for lattice specific heat in the simplest approximation,

$$C_L = \alpha T^3, \tag{1}$$

and then extrapolated it to lower temperature. The Schottky specific heat $C_S(\Delta)$ is given by

$$C_S(\Delta) = 3fR\left(\frac{\Delta}{k_B T}\right)^2 \frac{\exp\left(\frac{\Delta}{k_B T}\right)}{\left[1+\exp\left(\frac{\Delta}{k_B T}\right)\right]^2}. \tag{2}$$

The factor of 3 indicates that there are three Yb^{3+} ions in a formula unit. Here, f denotes the fraction of Yb^{3+} spins participating in the splitting of the ground state. This value is close to 1 ($f > 0.9$ for fields $\mu_0 H > 3$ T), indicating that almost all the spins are contributing to the specific heat. It is worth mentioning that, for transition metal oxides, f denotes the fraction of orphan or defect spins (5%–10%) that are present in the system owing to disorder [12,71]. It is found that the value of Δ increases with an external applied magnetic field typical for many frustrated magnetic materials [39,65]. The Landé g factor turns out to be 3.3(1) from the slope of the linear fit to the Δ/k_B vs $\mu_0 H$ plot [see Fig. 5(c)], which is consistent with the result obtained from magnetization data. We get a small zero-field splitting of 0.2(1) K from the intercept of the extrapolated linear fit. However, the deviation of the zero-field data from the Schottky specific heat indicates that the peak around 200 mK might be due to the presence of short-range spin correlation between Yb^{3+} ions in this 3D spin lattice. It is worth mentioning that a crystal electric field can also split the energy levels and give rise to a Schottky-type anomaly. However, the energy difference from the ground state to the first excited state in most rare-earth materials is of the order of 5 meV or more, which corresponds to a temperature of 58 K [23,47,72,73]. Magnetic specific heat C_m was obtained after subtracting the lattice (C_L) and nuclear [$C_N(^{171}\text{Yb} + {}^{173}\text{Yb})$] contributions to the specific heat from the raw specific heat data C_p in the entire temperature range. However, we did not subtract the nuclear contribution for higher field data because our lowest accessible temperature in applied field is 0.5 K, where the nuclear contribution is almost negligible [i.e., 0.026 J/(mol K)]. The magnetic entropy can shed light on the ground state properties of frustrated magnetic materials. We have extracted the entropy by integrating C_m/T from the lowest accessible temperature (130 mK for zero field) to 20 K, and the results are shown in Fig. 5(d). Due to experimental limitations in accessing temperature below 130 mK, the zero-field specific heat is not fully recovered, yielding a lower value of entropy than that expected for spin half magnetic materials. The zero-field entropy does not saturate to $R \ln 2$ even up to 20 K. This residual entropy below 130 mK might indicate the role of magnetic frustration at very low temperature. However, in the application of a magnetic field, the entropy is dominated by the Schottky effect in Kramers doublet systems. The obtained high θ_{CW} temperature (−114 K), which indicates crystal field splitting of the ground state, is very large. We expect that the excited state doublets are well separated from the ground state, so we can describe the low-temperature properties by accounting for only the lowest $J_{eff} = \frac{1}{2}$ ground state. The entropy taken at 3 T saturates at a value of 5.6 J/(mol K), which is close to the full entropy of $R \ln 2$ [i.e., 5.76 J/(mol K)] for the $J_{eff} = \frac{1}{2}$ spin state. This suggests that the ground state of this three-dimensional spin lattice could be mapped with a low-energy effective $J_{eff} = \frac{1}{2}$ state at low temperature, which is consistent with magnetization results [74,75].

E. Crystal electric field calculations

We performed a combined fit of specific heat data measured at 1, 2, 3, 5, and 7 T as well as magnetic susceptibility data measured at 0.01, 0.1, 1, 3, and 5 T. According to Hund's rule, the ground state multiplet of the Yb^{3+} ion is $^2F_{7/2}$, which is in a crystal field split into four Kramers doublets composed of $|\pm m_J\rangle$ states [$m_J = (2n-1)/2$, where $n = 1$–4]. The composition of the four Kramers doublets directly depends on the CEF Hamiltonian, which can be written as

$$H_{CEF} = \sum_{i,j} B_j^i O_j^i, \tag{3}$$

where O_j^i are Stevens operators [76] and B_j^i are the corresponding scaling parameters. The relevant B_j^i (Table III) are determined by point symmetry at the Yb^{3+} site and, in general, comply with those determined for the isostructural compound $Yb_3Ga_5O_{12}$ [44]. Indeed, we obtained very good agreement with the data measured at the applied magnetic field [lines in Figs. 6(a) and 6(b)] for the derived CEF parameters (Table III) when considering the additional T^3 term for the specific heat, accounting for the phonon contribution at low temperatures. Finally, we calculated the corresponding magnetization curves $M(H)$ [lines in Fig. 6(c)]. The agreement of the simulation and experiment is quite reasonable

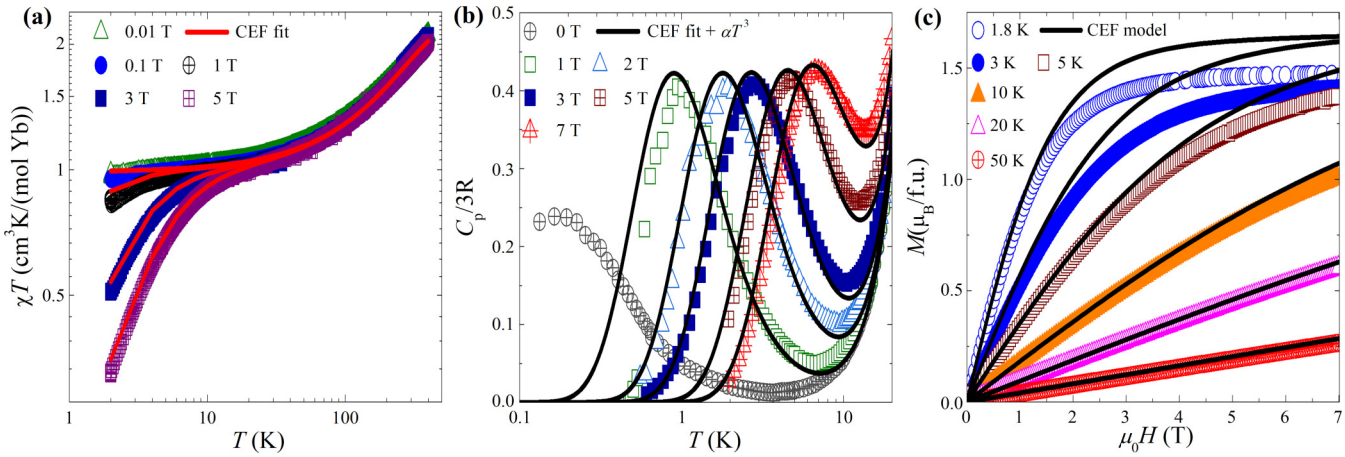

FIG. 6. (a) The temperature dependence of χT emphasizing the χ behavior at low temperatures. (b) The temperature dependence of specific heat measured in different magnetic fields. (c) Magnetization as a function of external magnetic field at several temperatures. Lines correspond to the CEF model presented in the text.

for both experiments. The derived magnetic anisotropy of the CEF ground state is determined by the g factor, which is also given in Table III, implying a rather uniaxial anisotropy, as g_z is considerably larger than g_x and g_y. In fact, the derived g values are in agreement with the average $g = 3.6$ derived from the ESR data measured at 20 K. All energy levels are summarized in Table IV, indicating that the ground state is well separated from the excited states, as found also in $Yb_3Ga_5O_{12}$ [44]. We note that the broad maximum in specific heat around 200 mK in zero field is clearly not related to CEF effects and, as suggested above, is most likely associated with the presence of short-range spin correlations.

III. DISCUSSION

The intertwining of spin-orbit coupling and electron correlation in frustrated magnets can stabilize exotic quantum states. In this context, rare-earth-based $4f$ frustrated magnets offer an exciting platform. In these materials, anisotropy and crystal electric field generated by the neighboring ligands govern the ground state properties. The choice of a suitable chemical element has a great role in tuning the crystal electric field, anisotropy, and exchange interaction and hence the ground state properties of rare-earth-based frustrated magnet. The hyperkagome material $Yb_3Sc_2Ga_3O_{12}$ belongs to the garnet family with cubic space group $Ia\bar{3}d$ and lattice constant $a = 12.391$ Å. Unlike $R_3Sc_2Ga_3O_{12}$ garnets (R = Tb, Dy, Ho), which order at low temperature, $Yb_3Sc_2Ga_3O_{12}$ does not show any long-range magnetic ordering at least down to 130 mK. This might be due to the low magnetic moment of Yb^{3+} and low exchange energy compared to other $R_3Sc_2Ga_3O_{12}$ compounds [40]. Furthermore, the absence of ZFC-FC splitting rules out spin freezing in this material. The small negative Curie-Weiss temperature indicates the presence of a weak antiferromagnetic interaction which arises mainly due to superexchange interaction. The values of Curie-Weiss temperature obtained from the fit of magnetic susceptibility data in high and low temperature regimes are comparable to those found in another Yb hyperkagome Li_3YbTeO_{12} [39]. ESR spectra taken for polycrystalline samples of $Yb_3Sc_2Ga_3O_{12}$ were found to be relatively broad, with a highly asymmetric shape which is related to magnetic anisotropy and most likely also to the distribution of Yb^{3+} moments [62]. The specific heat experiment, which is very sensitive to probe magnetic phase transition, ruled out a long-range magnetic order down to 130 mK in this frustrated magnet. The broad maximum around 200 mK in the specific heat data taken in zero field is ascribed to the development of short-range spin correlations at low temperature. The development of short-range spin correlations suggests the dominance of quantum effects at low temperature that lead to a dynamic liquidlike state in this 3D frustrated antiferromagnet. A similar broad maximum in specific heat at low temperature was also observed in the sister compound $Yb_3Ga_5O_{12}$ [45,66]. The low-temperature magnetic behavior can be described by the $J_{\text{eff}} = \frac{1}{2}$ Kramers doublet ground state as the energy levels of the excited Kramers doublets are well above the ground state, which was confirmed by our CEF calculations. This family of $R_3Sc_2Ga_3O_{12}$ rare-earth magnetic materials with a suitable choice of rare-earth and nonmagnetic cations has great potential to host nontrivial quantum states with exotic excitations.

TABLE IV. CEF energy levels (in meV) for the CEF model.

E_0	E_1	E_2	E_3
0	69	96	143

IV. CONCLUSION

In summary, we successfully synthesized and characterized a three-dimensional hyperkagome garnet, namely, $Yb_3Sc_2Ga_3O_{12}$. Magnetization data indicated the absence of long-range magnetic ordering and spin freezing down to 1.8 K. Specific heat measurements revealed that there is no long-range magnetic ordering down to 130 mK. A weak antiferromagnetic exchange interaction is present in this system, which is typical for rare-earth-based magnetic materials due

to the localized $4f$ moments. In addition, the absence of ZFC-FC splitting ruled out the formation of a glassy phase in this antiferromagnet. Our thermodynamic results indicated that the Yb^{3+} ions are in the Kramers doublet state with an effective $J_{\text{eff}} = \frac{1}{2}$ spin degree of freedom at low temperature. Furthermore, the ESR results indicated the existence of magnetic anisotropy. The presence of a broad maximum around 200 mK in the temperature dependence of specific heat suggests that short-range spin correlation phenomena at play in this frustrated magnet. Our CEF modeling suggested that the ground state is well separated from the excited states and yields very good agreement with thermodynamic and ESR results. Given the fact that the exchange interaction is weak in $4f$ systems, further low-temperature thermodynamic and muon spin relaxation experiments are required to track the ground state properties unambiguously. Microscopic experiments such as neutron scattering are desired to provide insights into the spin-orbit-driven anisotropy driving novel ground state arises from the crystal field splitting of the rare-earth multiplet. Understanding the spin anisotropy and low-energy spin excitation spectra provides an interesting way to reveal interesting insights into the ground state properties of this novel frustrated magnet. This family of rare-earth hyperkagome $R_3Sc_2Ga_3O_{12}$ (R = rare-earth) compounds offers a promising platform for the experimental realization of unconventional ground states born from spin correlation, frustration, and spin-orbit-driven anisotropy.

ACKNOWLEDGMENTS

P.K. acknowledges the funding from the Science and Engineering Research Board and Department of Science and Technology, India, through research grants. M.P. acknowledges the funding from the Slovenian Research and Innovation Agency (ARIS) (Project No. J2-2513 and Program No. P1-0125).

[1] H. T. Diep, *Frustrated Spin Systems* (World Scientific, Singapore, 2005).

[2] *Introduction to Frustrated Magnetism: Materials, Experiments, Theory*, edited by C. Lacroix, P. Mendels, and F. Mila, Springer Series in Solid-State Sciences Vol. 164 (Springer, Berlin, 2011).

[3] L. Savary and L. Balents, Quantum spin liquids: A review, Rep. Prog. Phys. **80**, 016502 (2017).

[4] Y. Zhou, K. Kanoda, and T.-K. Ng, Quantum spin liquid states, Rev. Mod. Phys. **89**, 025003 (2017).

[5] P. Anderson, Resonating valence bonds: A new kind of insulator?, Mater. Res. Bull. **8**, 153 (1973).

[6] L. Balents, Spin liquids in frustrated magnets, Nature (London) **464**, 199 (2010).

[7] S.-H. Do, S.-Y. Park, J. Yoshitake, J. Nasu, Y. Motome, Y. Kwon, D. T. Adroja, D. J. Voneshen, K. Kim, T.-H. Jang, J.-H. Park, K.-Y. Choi, and S. Ji, Majorana fermions in the Kitaev quantum spin system α-$RuCl_3$, Nat. Phys. **13**, 1079 (2017).

[8] A. Banerjee, C. A. Bridges, J.-Q. Yan, A. A. Aczel, L. Li, M. B. Stone, G. E. Granroth, M. D. Lumsden, Y. Yiu, J. Knolle, S. Bhattacharjee, D. L. Kovrizhin, R. Moessner, D. A. Tennant, D. G. Mandrus, and S. E. Nagler, Proximate Kitaev quantum spin liquid behaviour in a honeycomb magnet, Nat. Mater. **15**, 733 (2016).

[9] C. Broholm, R. J. Cava, S. A. Kivelson, D. G. Nocera, M. R. Norman, and T. Senthil, Quantum spin liquids, Science **367**, eaay0668 (2020).

[10] Y. Shimizu, K. Miyagawa, K. Kanoda, M. Maesato, and G. Saito, Spin liquid state in an organic Mott insulator with a triangular lattice, Phys. Rev. Lett. **91**, 107001 (2003).

[11] T. Itou, A. Oyamada, S. Maegawa, M. Tamura, and R. Kato, Quantum spin liquid in the spin-1/2 triangular antiferromagnet $EtMe_3Sb[Pd(dmit)_2]_2$, Phys. Rev. B **77**, 104413 (2008).

[12] H. D. Zhou, E. S. Choi, G. Li, L. Balicas, C. R. Wiebe, Y. Qiu, J. R. D. Copley, and J. S. Gardner, Spin liquid state in the $S = 1/2$ triangular lattice $Ba_3CuSb_2O_9$, Phys. Rev. Lett. **106**, 147204 (2011).

[13] P. Khuntia, R. Kumar, A. V. Mahajan, M. Baenitz, and Y. Furukawa, Spin liquid state in the disordered triangular lattice $Sc_2Ga_2CuO_7$ revealed by NMR, Phys. Rev. B **93**, 140408(R) (2016).

[14] M. P. Shores, E. A. Nytko, B. M. Bartlett, and D. G. Nocera, A structurally perfect S = 1/2 kagome antiferromagnet, J. Am. Chem. Soc. **127**, 13462 (2005).

[15] A. Olariu, P. Mendels, F. Bert, F. Duc, J. C. Trombe, M. A. de Vries, and A. Harrison, ^{17}O NMR study of the intrinsic magnetic susceptibility and spin dynamics of the quantum kagome antiferromagnet $ZnCu_3(OH)_6Cl_2$, Phys. Rev. Lett. **100**, 087202 (2008).

[16] P. Khuntia, M. Velazquez, Q. Barthélemy, F. Bert, E. Kermarrec, A. Legros, B. Bernu, L. Messio, A. Zorko, and P. Mendels, Gapless ground state in the archetypal quantum kagome antiferromagnet $ZnCu_3(OH)_6Cl_2$, Nat. Phys. **16**, 469 (2020).

[17] Y. Li, H. Liao, Z. Zhang, S. Li, F. Jin, L. Ling, L. Zhang, Y. Zou, L. Pi, Z. Yang, J. Wang, Z. Wu, and Q. Zhang, Gapless quantum spin liquid ground state in the two-dimensional spin-1/2 triangular antiferromagnet $YbMgGaO_4$, Sci. Rep. **5**, 16419 (2015).

[18] Y. Li, D. Adroja, R. I. Bewley, D. Voneshen, A. A. Tsirlin, P. Gegenwart, and Q. Zhang, Crystalline electric-field randomness in the triangular lattice spin-liquid $YbMgGaO_4$, Phys. Rev. Lett. **118**, 107202 (2017).

[19] Y. Li, S. Bachus, B. Liu, I. Radelytskyi, A. Bertin, A. Schneidewind, Y. Tokiwa, A. A. Tsirlin, and P. Gegenwart, Rearrangement of uncorrelated valence bonds evidenced by low-energy spin excitations in $YbMgGaO_4$, Phys. Rev. Lett. **122**, 137201 (2019).

[20] I. Kimchi, A. Nahum, and T. Senthil, Valence bonds in random quantum magnets: theory and application to $YbMgGaO_4$, Phys. Rev. X **8**, 031028 (2018).

[21] H. Takagi, T. Takayama, G. Jackeli, G. Khaliullin, and S. E. Nagler, Concept and realization of Kitaev quantum spin liquids, Nat. Rev. Phys. **1**, 264 (2019).

[22] L. Clark, G. Sala, D. D. Maharaj, M. B. Stone, K. S. Knight, M. T. F. Telling, X. Wang, X. Xu, J. Kim, Y. Li, S.-W. Cheong, and B. D. Gaulin, Two-dimensional spin liquid behaviour in the

triangular-honeycomb antiferromagnet $TbInO_3$, Nat. Phys. **15**, 262 (2019).

[23] T. Arh, B. Sana, M. Pregelj, P. Khuntia, Z. Jagličić, M. D. Le, P. K. Biswas, P. Manuel, L. Mangin-Thro, A. Ozarowski, and A. Zorko, The ising triangular-lattice antiferromagnet neodymium heptatantalate as a quantum spin liquid candidate, Nat. Mater. **21**, 416 (2022).

[24] B. Koteswararao, R. Kumar, P. Khuntia, S. Bhowal, S. K. Panda, M. R. Rahman, A. V. Mahajan, I. Dasgupta, M. Baenitz, K. H. Kim, and F. C. Chou, Magnetic properties and heat capacity of the three-dimensional frustrated $S = \frac{1}{2}$ antiferromagnet $PbCuTe_2O_6$, Phys. Rev. B **90**, 035141 (2014).

[25] P. Khuntia, F. Bert, P. Mendels, B. Koteswararao, A. V. Mahajan, M. Baenitz, F. C. Chou, C. Baines, A. Amato, and Y. Furukawa, Spin liquid state in the 3D frustrated antiferromagnet $PbCuTe_2O_6$: NMR and muon spin relaxation studies, Phys. Rev. Lett. **116**, 107203 (2016).

[26] S. Chillal, Y. Iqbal, H. O. Jeschke, J. A. Rodriguez-Rivera, R. Bewley, P. Manuel, D. Khalyavin, P. Steffens, R. Thomale, A. T. M. N. Islam, J. Reuther, and B. Lake, Evidence for a three-dimensional quantum spin liquid in $PbCuTe_2O_6$, Nat. Commun. **11**, 2348 (2020).

[27] C. Balz, B. Lake, J. Reuther, H. Luetkens, R. Schönemann, T. Herrmannsdörfer, Y. Singh, A. T. M. Nazmul Islam, E. M. Wheeler, J. Rodriguez-Rivera, T. Guidi, G. Simeoni, C. Baines, and H. Ryll, Physical realization of a quantum spin liquid based on a complex frustration mechanism, Nat. Phys. **12**, 942 (2016).

[28] C. Balz, B. Lake, A. T. M. Nazmul Islam, Y. Singh, J. A. Rodriguez-Rivera, T. Guidi, E. M. Wheeler, G. G. Simeoni, and H. Ryll, Magnetic Hamiltonian and phase diagram of the quantum spin liquid $Ca_{10}Cr_7O_{28}$, Phys. Rev. B **95**, 174414 (2017).

[29] K. W. Plumb, H. J. Changlani, A. Scheie, S. Zhang, J. W. Krizan, J. A. Rodriguez-Rivera, Y. Qiu, B. Winn, R. J. Cava, and C. L. Broholm, Continuum of quantum fluctuations in a three-dimensional S = 1 Heisenberg magnet, Nat. Phys. **15**, 54 (2019).

[30] B. Gao *et al.*, Experimental signatures of a three-dimensional quantum spin liquid in effective spin-1/2 $Ce_2Zr_2O_7$ pyrochlore, Nat. Phys. **15**, 1052 (2019).

[31] J. Gaudet, E. M. Smith, J. Dudemaine, J. Beare, C. R. C. Buhariwalla, N. P. Butch, M. B. Stone, A. I. Kolesnikov, G. Xu, D. R. Yahne, K. A. Ross, C. A. Marjerrison, J. D. Garrett, G. M. Luke, A. D. Bianchi, and B. D. Gaulin, Quantum spin ice dynamics in the dipole-octupole pyrochlore magnet $Ce_2Zr_2O_7$, Phys. Rev. Lett. **122**, 187201 (2019).

[32] Y.-D. Li and G. Chen, Symmetry enriched U(1) topological orders for dipole-octupole doublets on a pyrochlore lattice, Phys. Rev. B **95**, 041106(R) (2017).

[33] E. M. Smith *et al.*, Case for a $U(1)_\pi$ quantum spin liquid ground state in the dipole-octupole pyrochlore $Ce_2Zr_2O_7$, Phys. Rev. X **12**, 021015 (2022).

[34] Y. Okamoto, M. Nohara, H. Aruga-Katori, and H. Takagi, Spin -liquid state in the $S = 1/2$ hyperkagome antiferromagnet $Na_4Ir_3O_8$, Phys. Rev. Lett. **99**, 137207 (2007).

[35] Y. Zhou, P. A. Lee, T.-K. Ng, and F.-C. Zhang, $Na_4Ir_3O_8$ as a 3D spin liquid with fermionic spinons, Phys. Rev. Lett. **101**, 197201 (2008).

[36] M. J. Lawler, H.-Y. Kee, Y. B. Kim, and A. Vishwanath, Topological spin liquid on the hyperkagome lattice of $Na_4Ir_3O_8$, Phys. Rev. Lett. **100**, 227201 (2008).

[37] A. C. Shockley, F. Bert, J.-C. Orain, Y. Okamoto, and P. Mendels, Frozen state and spin liquid physics in $Na_4Ir_3O_8$: an NMR study, Phys. Rev. Lett. **115**, 047201 (2015).

[38] D. I. Khomskii, *Transition Metal Compounds* (Cambridge University Press, Cambridge, 2014).

[39] J. Khatua, S. Bhattacharya, Q. P. Ding, S. Vrtnik, A. M. Strydom, N. P. Butch, H. Luetkens, E. Kermarrec, M. S. Ramachandra Rao, A. Zorko, Y. Furukawa, and P. Khuntia, Spin liquid state in a rare-earth hyperkagome lattice, Phys. Rev. B **106**, 104404 (2022).

[40] P. Mukherjee, A. C. S. Hamilton, H. F. J. Glass, and S. E. Dutton, Sensitivity of magnetic properties to chemical pressure in lanthanide garnets $Ln_3A_2X_3O_{12}$, Ln = Gd, Tb, Dy, Ho, A = Ga, Sc, In, Te, X = Ga, Al, Li, J. Phys.: Condens. Matter **29**, 405808 (2017).

[41] J. A. M. Paddison, H. Jacobsen, O. A. Petrenko, M. T. Fernández-Díaz, P. P. Deen, and A. L. Goodwin, Hidden order in spin-liquid $Gd_3Ga_5O_{12}$, Science **350**, 179 (2015).

[42] H. Jacobsen, O. Florea, E. Lhotel, K. Lefmann, O. A. Petrenko, C. S. Knee, T. Seydel, P. F. Henry, R. Bewley, D. Voneshen, A. Wildes, G. Nilsen, and P. P. Deen, Spin dynamics of the director state in frustrated hyperkagome systems, Phys. Rev. B **104**, 054440 (2021).

[43] Y. Machida, S. Nakatsuji, S. Onoda, T. Tayama, and T. Sakakibara, Time-reversal symmetry breaking and spontaneous Hall effect without magnetic dipole order, Nature (London) **463**, 210 (2010).

[44] L. Ø. Sandberg, R. Edberg, I.-M. B. Bakke, K. S. Pedersen, M. C. Hatnean, G. Balakrishnan, L. Mangin-Thro, A. Wildes, B. Fåk, G. Ehlers, G. Sala, P. Henelius, K. Lefmann, and P. P. Deen, Emergent magnetic behavior in the frustrated $Yb_3Ga_5O_{12}$ garnet, Phys. Rev. B **104**, 064425 (2021).

[45] P. Dalmas de Réotier, A. Yaouanc, P. C. M. Gubbens, C. T. Kaiser, C. Baines, and P. J. C. King, Absence of magnetic order in $Yb_3Ga_5O_{12}$: relation between phase transition and entropy in geometrically frustrated materials, Phys. Rev. Lett. **91**, 167201 (2003).

[46] J. A. Hodges, P. Bonville, M. Rams, and K. Królas, Low-temperature spin fluctuations in geometrically frustrated $Yb_3Ga_5O_{12}$, J. Phys.: Condens. Matter **15**, 4631 (2003).

[47] Y. Cai, M. N. Wilson, J. Beare, C. Lygouras, G. Thomas, D. R. Yahne, K. Ross, K. M. Taddei, G. Sala, H. A. Dabkowska, A. A. Aczel, and G. M. Luke, Crystal fields and magnetic structure of the Ising antiferromagnet $Er_3Ga_5O_{12}$, Phys. Rev. B **100**, 184415 (2019).

[48] N. Zhao, H. Ge, L. Zhou, Z. M. Song, J. Yang, T. T. Li, L. Wang, Y. Fu, Y. F. Zhang, J. B. Xu, S. M. Wang, J. W. Mei, X. Tong, L. S. Wu, and J. M. Sheng, Antiferromagnetism and Ising ground states in the rare-earth garnet $Nd_3Ga_5O_{12}$, Phys. Rev. B **105**, 014441 (2022).

[49] N. F. Chilton, R. P. Anderson, L. D. Turner, A. Soncini, and K. S. Murray, PHI: A powerful new program for the analysis of anisotropic monomeric and exchange-coupled polynuclear d-and f-block complexes, J. Comput. Chem. **34**, 1164 (2013).

[50] J. Rodríguez-Carvajal, Recent advances in magnetic structure determination by neutron powder diffraction, Phys. B (Amsterdam, Neth.) **192**, 55 (1993).

[51] K. Momma and F. Izumi, *VESTA3* for three-dimensional visualization of crystal, volumetric and morphology data, J. Appl. Crystallogr. **44**, 1272 (2011).

[52] See Supplemental Material at http://link.aps.org/supplemental/10.1103/PhysRevB.108.134413 for the validity of the Curie-Weiss law in different temperature regimes, variation of the Curie-Weiss temperature for different temperature regimes, the hysteresis curve taken at 1.8 K, and the model used to calculate the nuclear Schottky specific heat (see also Refs. [77–84] therein).

[53] R. A. Buchanan, K. A. Wickersheim, J. J. Pearson, and G. F. Herrmann, Energy Levels of Yb^{3+} in Gallium and Aluminum Garnets. I. Spectra, Phys. Rev. **159**, 245 (1967).

[54] V. Simonet, R. Ballou, J. Robert, B. Canals, F. Hippert, P. Bordet, P. Lejay, P. Fouquet, J. Ollivier, and D. Braithwaite, Hidden magnetic frustration by quantum relaxation in anisotropic Nd langasite, Phys. Rev. Lett. **100**, 237204 (2008).

[55] Y. Shen, Y.-D. Li, H. Wo, Y. Li, S. Shen, B. Pan, Q. Wang, H. C. Walker, P. Steffens, M. Boehm, Y. Hao, D. L. Quintero-Castro, L. W. Harriger, M. D. Frontzek, L. Hao, S. Meng, Q. Zhang, G. Chen, and J. Zhao, Evidence for a spinon Fermi surface in a triangular-lattice quantum-spin-liquid candidate, Nature (London) **540**, 559 (2016).

[56] E. Lhotel, L. Mangin-Thro, E. Ressouche, P. Steffens, E. Bichaud, G. Knebel, J.-P. Brison, C. Marin, S. Raymond, and M. E. Zhitomirsky, Spin dynamics of the quantum dipolar magnet $Yb_3Ga_5O_{12}$ in an external field, Phys. Rev. B **104**, 024427 (2021).

[57] J. Jensen and A. R. Mackintosh, *Rare Earth Magnetism: Structures and Excitations* (Clarendon, Oxford, 1991).

[58] S. S. Sosin, A. F. Iafarova, I. V. Romanova, O. A. Morozov, S. L. Korableva, R. G. Batulin, M. Zhitomirsky, and V. N. Glazkov, Microscopic spin Hamiltonian for a dipolar Heisenberg magnet $LiGdF_4$ from EPR measurements, JETP Lett. **116**, 771 (2022).

[59] A. C. S. Hamilton, G. I. Lampronti, S. E. Rowley, and S. E. Dutton, Enhancement of the magnetocaloric effect driven by changes in the crystal structure of Al-doped GGG, $Gd_3Ga_{5-x}Al_xO_{12}(0 \leqslant x \leqslant 5)$, J. Phys.: Condens. Matter **26**, 116001 (2014).

[60] Z.-X. Luo, E. Lake, J.-W. Mei, and O. A. Starykh, Spinon magnetic resonance of quantum spin liquids, Phys. Rev. Lett. **120**, 037204 (2018).

[61] K. Somesh, S. S. Islam, S. Mohanty, G. Simutis, Z. Guguchia, C. Wang, J. Sichelschmidt, M. Baenitz, and R. Nath, Absence of magnetic order and emergence of unconventional fluctuations in the $J_{\text{eff}} = \frac{1}{2}$ triangular-lattice antiferromagnet $YbBO_3$, Phys. Rev. B **107**, 064421 (2023).

[62] H. Benner, M. Brodehl, H. Seitz, and J. Wiese, Influence of nondiagonal dynamic susceptibility on the EPR signal of Heisenberg magnets, J. Phys. C **16**, 6011 (1983).

[63] A. Tari, *The Specific Heat of Matter at Low Temperatures* (Imperial College Press, London, 2003).

[64] E. Gopal, *Specific Heats at Low Temperatures* (Springer, New York, 2012).

[65] C. Y. Jiang, Y. X. Yang, Y. X. Gao, Z. T. Wan, Z. H. Zhu, T. Shiroka, C. S. Chen, Q. Wu, X. Li, J. C. Jiao, K. W. Chen, Y. Bao, Z. M. Tian, and L. Shu, Spin excitations in the quantum dipolar magnet $Yb(BaBO_3)_3$, Phys. Rev. B **106**, 014409 (2022).

[66] J. Filippi, J. C. Lasjaunias, B. Hebral, J. Rossat-Mignod, and F. Tcheou, Magnetic properties of ytterbium gallium garnet between 44 mK and 4 K, J. Phys. C **13**, 1277 (1980).

[67] O. V. Lounasmaa, Specific heat of holmium metal between 0.38 and 4.2°K, Phys. Rev. **128**, 1136 (1962).

[68] Y. Takeda, N. Duc Dung, Y. Nakano, T. Ishikura, S. Ikeda, T. D. Matsuda, E. Yamamoto, Y. Haga, T. Takeuchi, R. Settai, and Y. Ōnuki, Calorimetric study in single crystalline RCu_2Si_2 (R: rare earth), J. Phys. Soc. Jpn. **77**, 104710 (2008).

[69] S. Kundu, A. Shahee, A. Chakraborty, K. M. Ranjith, B. Koo, J. Sichelschmidt, M. T. F. Telling, P. K. Biswas, M. Baenitz, I. Dasgupta, S. Pujari, and A. V. Mahajan, Gapless quantum spin liquid in the triangular system $Sr_3CuSb_2O_9$, Phys. Rev. Lett. **125**, 267202 (2020).

[70] T. Dey, A. V. Mahajan, P. Khuntia, M. Baenitz, B. Koteswararao, and F. C. Chou, Spin-liquid behavior in $J_{\text{eff}} = \frac{1}{2}$ triangular lattice compound $Ba_3IrTi_2O_9$, Phys. Rev. B **86**, 140405(R) (2012).

[71] M. A. de Vries, K. V. Kamenev, W. A. Kockelmann, J. Sanchez-Benitez, and A. Harrison, Magnetic ground state of an experimental $S = 1/2$ kagome antiferromagnet, Phys. Rev. Lett. **100**, 157205 (2008).

[72] J. A. M. Paddison, M. Daum, Z. Dun, G. Ehlers, Y. Liu, M. Stone, H. Zhou, and M. Mourigal, Continuous excitations of the triangular-lattice quantum spin liquid $YbMgGaO_4$, Nat. Phys. **13**, 117 (2017).

[73] M. Baenitz, P. Schlender, J. Sichelschmidt, Y. A. Onykiienko, Z. Zangeneh, K. M. Ranjith, R. Sarkar, L. Hozoi, H. C. Walker, J.-C. Orain, H. Yasuoka, J. van den Brink, H. H. Klauss, D. S. Inosov, and T. Doert, $NaYbS_2$: A planar spin-$\frac{1}{2}$ triangular-lattice magnet and putative spin liquid, Phys. Rev. B **98**, 220409(R) (2018).

[74] S. Yamashita, Y. Nakazawa, M. Oguni, Y. Oshima, H. Nojiri, Y. Shimizu, K. Miyagawa, and K. Kanoda, Thermodynamic properties of a spin-1/2 spin-liquid state in a κ-type organic salt, Nat. Phys. **4**, 459 (2008).

[75] S. Yamashita, T. Yamamoto, Y. Nakazawa, M. Tamura, and R. Kato, Gapless spin liquid of an organic triangular compound evidenced by thermodynamic measurements, Nat. Commun. **2**, 275 (2011).

[76] K. W. H. Stevens, Matrix elements and operator equivalents connected with the magnetic properties of rare earth ions, Proc. Phys. Soc. London, Sect. A **65**, 209 (1952).

[77] B. Schmidt, J. Sichelschmidt, K. M. Ranjith, T. Doert, and M. Baenitz, Yb delafossites: Unique exchange frustration of $4f$ spin-$\frac{1}{2}$ moments on a perfect triangular lattice, Phys. Rev. B **103**, 214445 (2021).

[78] E. Grivei, V. Bayot, L. Piraux, and J.-P. Issi, Nuclear Schottky effect in thulium, Phys. Rev. B **51**, 1301 (1995).

[79] R. Movshovich, A. Yatskar, M. F. Hundley, P. C. Canfield, and W. P. Beyermann, Magnetic-field dependence of the low-temperature specific heat in $PrInAg_2$: Support for a nonmagnetic heavy-fermion ground state, Phys. Rev. B **59**, R6601 (1999).

[80] M. J. P. Gingras, B. C. den Hertog, M. Faucher, J. S. Gardner, S. R. Dunsiger, L. J. Chang, B. D. Gaulin, N. P. Raju, and J. E. Greedan, Thermodynamic and single-ion properties of Tb^{3+} within the collective paramagnetic-spin liquid state of the

frustrated pyrochlore antiferromagnet $Tb_2Ti_2O_7$, Phys. Rev. B **62**, 6496 (2000).

[81] E. Bauer, R. Lackner, G. Hilscher, H. Michor, E.-W. Scheidt, W. Scherer, P. Rogl, A. Gribanov, A. Tursina, Y. Seropegin, and G. Giester, Crystal chemistry and low-temperature properties of $Yb_{18}Pt_{51.1}Si_{15.1}$($\approx$ $YbPt_3Si$), Phys. Rev. B **73**, 104405 (2006).

[82] S. K. Dhar, R. Kulkarni, P. Manfrinetti, M. Pani, Y. Yonezawa, and Y. Aoki, Synthesis, crystal structure, and physical properties of YbTZn (T = Pd, Pt, and Au) and LuPtZn, Phys. Rev. B **76**, 054411 (2007).

[83] A. M. Hallas, J. Gaudet, N. P. Butch, M. Tachibana, R. S. Freitas, G. M. Luke, C. R. Wiebe, and B. D. Gaulin, Universal dynamic magnetism in Yb pyrochlores with disparate ground states, Phys. Rev. B **93**, 100403(R) (2016).

[84] A. Steppke, M. Brando, N. Oeschler, C. Krellner, C. Geibel, and F. Steglich, Nuclear contribution to the specific heat of $Yb(Rh_{0.93}Co_{0.07})_2Si_2$, Phys. Status Solidi B **247**, 737 (2010).